Program Digest, 2019 IEEE International Ultrasonics Symposium (IUS)
Glasgow, Scotland, October 6-9, 2019

High Quality Ultrafast Imaging with Transmit Extrapolation

Junseob Shin
Philips Research North America
Cambridge, MA, USA
junseob.shin@philips.com

Francois Vignon
Philips Research North America
Cambridge, MA, USA
francois.vignon@philips.com

Sheng-Wen Huang
Philips Research North America
Cambridge, MA, USA
sheng-wen.huang@philips.com

Jean-luc Robert
Philips Research North America
Cambridge, MA, USA
jean-luc.robert@philips.com

Abstract— **Plane wave imaging (PWI) and diverging wave imaging (DWI) can achieve high frame rate by coherently compounding beamsum data from broad transmit beams at different angles. However, many transmits are still needed as image quality degradation occurs with reduced number of transmit angles in PWI/DWI. Specifically, a reduced transmit angular span results in degraded lateral resolution in the synthetic transmit beam. We propose a transmit extrapolation (TEX) technique, which employs a linear prediction scheme to predict unavailable beamsum data based on beamsum data available from a limited number and span of PW/DW transmit angles. The original and predicted beamsum data are then coherently compounded to achieve image quality superior to that with only the original beamsum data, thereby overcoming the inherent trade-off between frame rate and image quality. We evaluate our TEX technique on the PICMUS dataset. Our results suggest that TEX has potential to enable ultrafast imaging without compromising image quality.**

Keywords—beamforming, ultrafast imaging, transmit extrapolation, autoregressive model

I. INTRODUCTION

Plane wave imaging (PWI), or diverging waves imaging (DWI) in the case of phased arrays, is a relatively new imaging technique that enables imaging at much higher frame rates than was previously the norm [1]. It has also opened up many new imaging modes for different applications which were previously not possible with conventional imaging with focused transmit beams. For this reason, PWI/DWI has been one of the most active areas of research in the past few years.

PWI achieves a two-way focused, high-quality image by coherently compounding images obtained from PW transmissions at different steering angles. According to [1] and [2], the total number of transmit steering angles, N, in the complete PW angle sequence to achieve the same image quality as the conventional imaging with focused transmits is a function of the aperture width L, the F-number $F_{\#}$, and the wavelength λ:

$$N = \frac{L}{F_{\#}\lambda} \tag{1}$$

The complete angle span consists of N steering angles over [-α_{max}, α_{max}] = $[-\frac{1}{2F_{\#}}, \frac{1}{2F_{\#}}]$. From (1), it can be shown that $F_{\#}$, and thus, the resolution is only a function of the maximum angle used α_{max} and not the total angle sequence:

$$F_{\#} = \frac{L}{N\lambda} \approx \frac{1}{N\Delta\alpha} = \frac{1}{2\alpha_{max}}\frac{N-1}{N} \approx \frac{1}{2\alpha_{max}} \tag{2}$$

This implies that the frame rate can be improved without losing resolution in PWI by decimating the angle sequence and maintaining the maximum angle α_{max}. However, the trade-off in this approach is reduced image contrast due to grating lobes as a result of underdamping of the spatial frequencies. Many, if not most, of the recent advanced beamforming algorithms in the context of high frame-rate PWI uses the decimated transmit angle scheme [3-5].

In addition, PWI may suffer from motion artifacts particularly when imaging fast-moving organs as motion may cause imperfect registration between different PW transmissions. The effect of motion becomes more severe with increasing number of PW transmissions. Thus, there is another apparent trade-off in PWI: more transmit angles are needed to achieve high image quality, but in practice, more transmit angles make it more susceptible to motion which degrades image quality.

Lastly, regardless of the number of transmit angles, PWI does not reduce multipath reverberation clutter artifacts, which is one of the main sources of image quality degradation in fundamental B-mode images *in vivo* [6].

In order to overcome these limitations, we propose a transmit extrapolation (TEX) technique, which, based on beamsum data from only a few center transmit angles, predicts beamsum data from other transmit angles that have not been acquired. The original and predicted data are then coherently compounded together to form the final image. This technique allows for ultrafast imaging with 1) no transmit grating lobes, 2) improved spatial resolution compared to the image from original transmit angles, 3) improved image contrast by reducing multipath clutter that is not predicted by the extrapolation, and 4) reduced motion artifacts compared to image from real PW transmissions corresponding to original and predicted combined. In this work, we focus on presenting our initial results and analysis for 1) - 3).

II. METHODS

A. Linear Prediction

In linear prediction, the current signal sample x_m in $\boldsymbol{x} = [x_1, x_2, \ldots, x_M]^{\mathrm{T}}$ is approximated as a linear combination of p previous samples using a finite impulse response (FIR) filter:

$$\tilde{x}_m = \sum_{j=1}^{p} x_{m-j} a_j \tag{3}$$

where a_j are the prediction filter coefficients. This process is also known as autoregression (AR) of order p. The prediction error between the actual sample x_m and the predicted sample $\tilde{x}_m$ is written as:

$$e_m = x_m - \tilde{x}_m = x_m - \sum_{j=1}^{p} x_{m-j} a_j \quad (4)$$

There are several approaches to compute a_j. The simplest approach is the least squares minimization of the mean-squared prediction error. In practice, the well-known Burg's maximum entropy method [7] is the preferred estimator of the AR parameters as it always produces a stable model [8]. This algorithm minimizes the forward and backward prediction errors with a constraint that the AR coefficients satisfy the Levinson recursion.

B. Transmit Extrapolation (TEX)

The proposed TEX technique is inspired by the work presented in [9] in which a linear prediction scheme was used in conjunction with narrowband line-array beamforming in underwater acoustics to achieve aperture extrapolation (APEX). While this concept may be employed to directly extrapolate the receive aperture when conventional focused transmit beams are used, we believe it is better suited for PWI/DWI which achieves two-way focusing in the entire field-of-view (FOV). In this work, we propose to adopt a similar approach for PWI/DWI and evaluate its benefits in terms of image quality.

The goal in TEX is to use an AR model to approximate the available beamsum data using only p most dominant spatial frequency components across different PW/DW transmits. An AR estimator, such as the Burg algorithm, can be utilized to estimate the AR coefficients that can be used to extrapolate beamsum data beyond available transmit angles. Readers interested in linear prediction theory and AR modeling may consult [10-11]. In this work, we focus our efforts on the TEX algorithm itself and evaluation of its performance.

For the m^{th} PW transmit in a linear array (or DW transmit in a phased array) with $m = 1, 2, \ldots, M$ where $M < N$, we acquire per-channel data and apply delay-and-sum (DAS) beamforming to obtain 2-dimensional beamsum data x_{su}, with scan lines $s = 1, 2, \ldots, S$ and axial samples $u = 1, 2, \ldots, U$. The PW beamsum data are obtained from the center M steering angles within the complete angle span consisting of N steering angles over $[-\alpha_{max}, \alpha_{max}] = [-\frac{1}{2F_\#}, \frac{1}{2F_\#}]$.

The main steps in TEX are depicted in Fig 1 and also summarized below:

1. For each scan line s, perform Fourier transform on a short axial segment of the beamsum signal from all M PW/DW steering angles. This transforms the time domain beamsum signal x_{mu} to X_{mv} in temporal frequency domain with $v = 1, 2, \ldots, V$.
2. For each temporal frequency within the transducer bandwidth, estimate the p^{th} order extrapolation filter coefficients (i.e. $a_1, a_2, \ldots, a_p$) via the Burg technique.
3. Since the actual temporal frequency v is not crucial in describing the algorithm, we omit the variable v for simplicity from here and regard the transmit angle index m as the primary variable. Using the p^{th} order extrapolation filter a_j, with $j = 1, 2, \ldots, p$, estimated in step 2 and the last p samples of the available transmit angles, $X_M, \ldots, X_{M-p}$, in the temporal frequency domain, apply a 1-step linear prediction extrapolator to obtain the 1st forward-extrapolated sample X_{M+1}:

$$X_{M+1} = \sum_{j=1}^{p} X_{M+1-j} a_j \quad (5)$$

Using the same approach, the 2nd forward-extrapolated sample X_{M+2} can be obtained with the 1st forward-extrapolated sample, X_{M+1} included in the calculation. By successively using this procedure, we can generate a desired number of new samples. This forward extrapolation process can be generalized and expressed as:

$$X_k = \sum_{j=1}^{p} X_{k-j} a_j\,, \quad k > M \quad (6)$$

Similarly, reverse the filter order and take the complex conjugate of the filter coefficients to backward-predict the value for the k^{th} transmit angle as a linear combination of the first p transmit angles:

$$X_k = \sum_{j=1}^{p} X_{k+j} a_j^*\,, \quad k < 1 \quad (7)$$

4. Perform inverse Fourier transform to transform the data back to the time domain. The beamsum data now consists of the original data and the extrapolated data on the left- and right-hand sides of the original data.
5. Repeat steps 1-4 at all axial depths.
6. Obtain the full extrapolated beamsum data and sum them all to obtain the coherently-compounded, high contrast beamsum data.

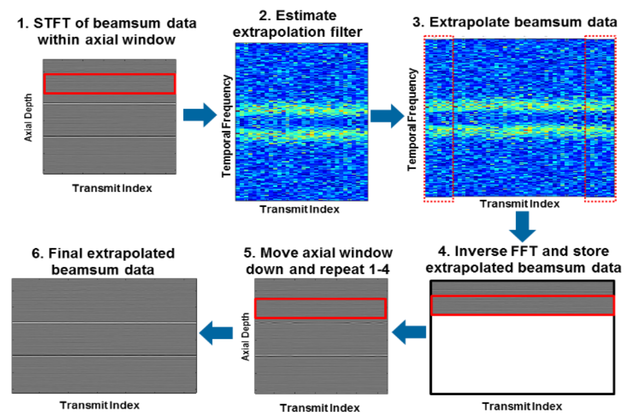

Fig 1. The main steps in the proposed TEX technique.

C. Simulation, Experimental, and In Vivo Data from PICMUS

For performance evaluation, we use the PICMUS dataset [12] which includes Field II simulation, experimental phantom, and *in vivo* data from human carotid. All data acquisitions are performed with a 128-element linear array with λ pitch, transmit center frequency of 5.2 MHz, aperture width of 38.4 mm and $F_\#$ = 1.75. More details are available in [12]. Each dataset consists of 75 PW transmissions with steering angles uniformly spaced between -16° and +16° at an interval of 0.43°, which is in agreement with (1) and (2). For all evaluations in this study, we use center 11 PWs between -2.16° and +2.16° (i.e. angle indices 33 to 43) rather than 11 PWs uniformly spaced between -16° and +16°. For TEX, we use $p = 5$ and an axial window of 5λ.

Performance is evaluated in terms of resolution and contrast as described in [12]. The axial and lateral resolutions are evaluated as the full width at half maximum (FWHM) of the point spread function (PSF) for all point targets and their average values are reported in Table I. For contrast, the contrast-to-noise ratio (CNR) [12] was computed for all anechoic cysts and their average values are reported in Table I.

III. Results and discussion

Fig 2 compares images from coherent compounding of center a) 11 PWs, b) 22 PWs, c) 44 PWs and from TEX with an extrapolation factor of d) 2 and e) 4 based on the original center 11 PWs. Results are shown for simulation (rows 1-2), experimental phantom (rows 3-4), and *in vivo* (row 5). The 22 PW and 44 PW cases are used to benchmark against TEX 2x and TEX 4x, respectively. The average resolution and contrast values are shown in Table I.

TABLE I. Comparison of Resolution and Contrast

	Simulation			**Experimental**		
	Average Resolution (mm)		*Average Contrast (dB)*	*Average Resolution (mm)*		*Average Contrast (dB)*
	Axial	*Lateral*		*Axial*	*Lateral*	
DAS 11PWs	0.40	0.81	11.46	0.57	0.87	8.55
DAS 22PWs	0.40	0.78	13.39	0.57	0.84	9.45
DAS 44PWs	0.40	0.69	15.27	0.56	0.70	10.95
TEX 2x	0.40	0.78	13.21	0.57	0.85	8.80
TEX 4x	0.41	0.68	14.18	0.58	0.73	9.25

For simulated point target results (Fig 2, row 1), the TEX 2x and TEX 4x images qualitatively match the images from coherently compounding true 22 PWs and 44 PWs, respectively. The lateral resolution improvement is visible in both cases while the axial resolution is unchanged. This is confirmed by the axial and lateral resolution values in Table I. For simulated anechoic cyst results (Fig 2, row 2), the TEX 2x and TEX 4x again achieve images qualitatively similar to the true 22-PW and 44-PW coherent compounding cases. The sidelobe clutter found in the anechoic cysts are reduced in both cases. This is confirmed by comparable average contrast values in Table I although TEX yields slightly lower contrast compared to their DAS counterparts. This is likely due to some speckle degradation that may have been caused by model mismatch in extrapolation filter estimation.

Similar patterns are observed with experimental phantom data for both resolution and contrast. The lateral resolution improves with TEX 2x and 4x by amount similar to the improvement observed with true 22 and 44 PWs (Fig 2, row 3), suggesting that the extrapolated beamsum data are highly accurate. The contrast from anechoic cyst targets (Fig 2, row 4) also improves with TEX 2x and 4x but lower than their DAS counterparts.

Lastly, the *in vivo* data (Fig 2, row 5) also shows contrast improvement associated with TEX 2x and 4x. In this case, multipath reverberation clutter, which presents itself as diffuse haze, is likely present in the data. Since such kind of acoustic noise is not modeled by AR process, TEX tends to suppress it. This explains why the carotid lumen looks much darker in the TEX images than in the true 22 and 44 PW images. The downside is that multipath clutter also degrades tissue signals, making the extrapolation process less reliable, especially with a higher extrapolation factor. This starts to become visible in the degraded speckle texture in the TEX 4x image.

IV. Conclusions and Future Work

In this work, we have presented a novel technique that can extrapolate beamsum data in PW transmit angles for ultrafast imaging. Our simulation and phantom results show that TEX improves lateral resolution and contrast by predicting the beamsum data from PW transmissions that have not occurred. We have shown that the TEX images (2x and 4x) with newly-predicted beamsum data are comparable to those obtained from the equivalent number of real PW transmissions. This suggests that TEX allows for at least a 2x or 4x frame rate improvement without compromising image quality. For future work, the robustness of the proposed technique in noisy environments will be studied and performance will be evaluated for DWI with phased arrays.

References

[1] G. Montaldo, M. Tanter, J. Bercoff, N. Benech, and M. Fink, “Coherent plane-wave compounding for very high frame rate ultrasonography and transient elastography”, *IEEE Trans. Ultrason., Ferroelectr., Freq. Control,* vol. 56, no. 3, pp. 489-506, Mar. 2009.

[2] B. Denarie, T. A. Tangen, I. K. Ekroll, N. Rolim, H. Torp, T. Bjastad, and L. Lovstakken, “Coherent plane wave compounding for very high frame rate ultrasonography of rapidly moving targets”, *IEEE Trans. Med. Imag,* vol. 32, no. 7, pp. 1265-1276, Jul. 2013.

[3] F. Matrone, A. S. Savoia, and G. Magenes, “Filtered delay multiply and sum beamforming in plane-wave ultrasound imaging: Tests on simulated and experimental data”, *Proc. IEEE Int. Ultrason. Symp., Sep. 2016.*

[4] T. Szasz, A. Basarab, and D. Kouame, “l_1-norm regularized beamforming in ultrasound imaging”, *Proc. IEEE Int. Ultrason. Symp., Sep. 2016.*

[5] T. Chernyakova, D. Cohen, M. Shoham, and Y. C. Eldar, “iMAP beamforming for high quality high frame rate image *IEEE Trans. Ultrason., Ferroelectr., Freq. Control,* Aug. 2019 (early access).

[6] G. F. Pinton, G. E. Trahey, and J. J. Dahl, “Sources of image degradation in fundamental and harmonic ultrasound imaging using nonlinear, full-wave simulations”, *IEEE Trans. Ultrason., Ferroelectr., Freq. Control,* vol. 58, no. 4, pp. 754-765, Apr. 2011.

[7] J. P. Burg, “Maximum entropy spectral analysis”, *In Proc. 37th Meet. Soc. Explorational Geophys.,* Oklahoma City, 1967.

[8] P. M. T. Broersen, “The ABC of autoregressive order selection criteria”, *In Proc. Sysid Conf.,* pp.231-236, Kitakyushu, Japan, 1997.

[9] D. N. Swingler and R. S. Walker, “Line-array beamforming using linear prediction for aperture interpolation and extrapolation”, *IEEE Trans. Acoust., Speech., Signal. Processing,* vol. 37, no. 1, pp. 16-30, Jan. 1989.

[10] P. Stoica and R. Moses, “Spectral analysis of signals”, Upper Saddle River, NJ: Prentice-Hall, 2005

[11] S. J. Orfanidis, “Applied optimum signal processing”, New York, NY: McGraw-Hill Publishing Compnay, 2007.

[12] H. Liebgott, A. Rodriguez-Molares, F. Cervenansky, J. A. Jensen, and O. Bernard, “Plane-wave imaging challenge in medical ultrasound”, in *Ultrasonics Symposium (ius), 2016 IEEE International.* IEEE, 2016, pp. 1-4.

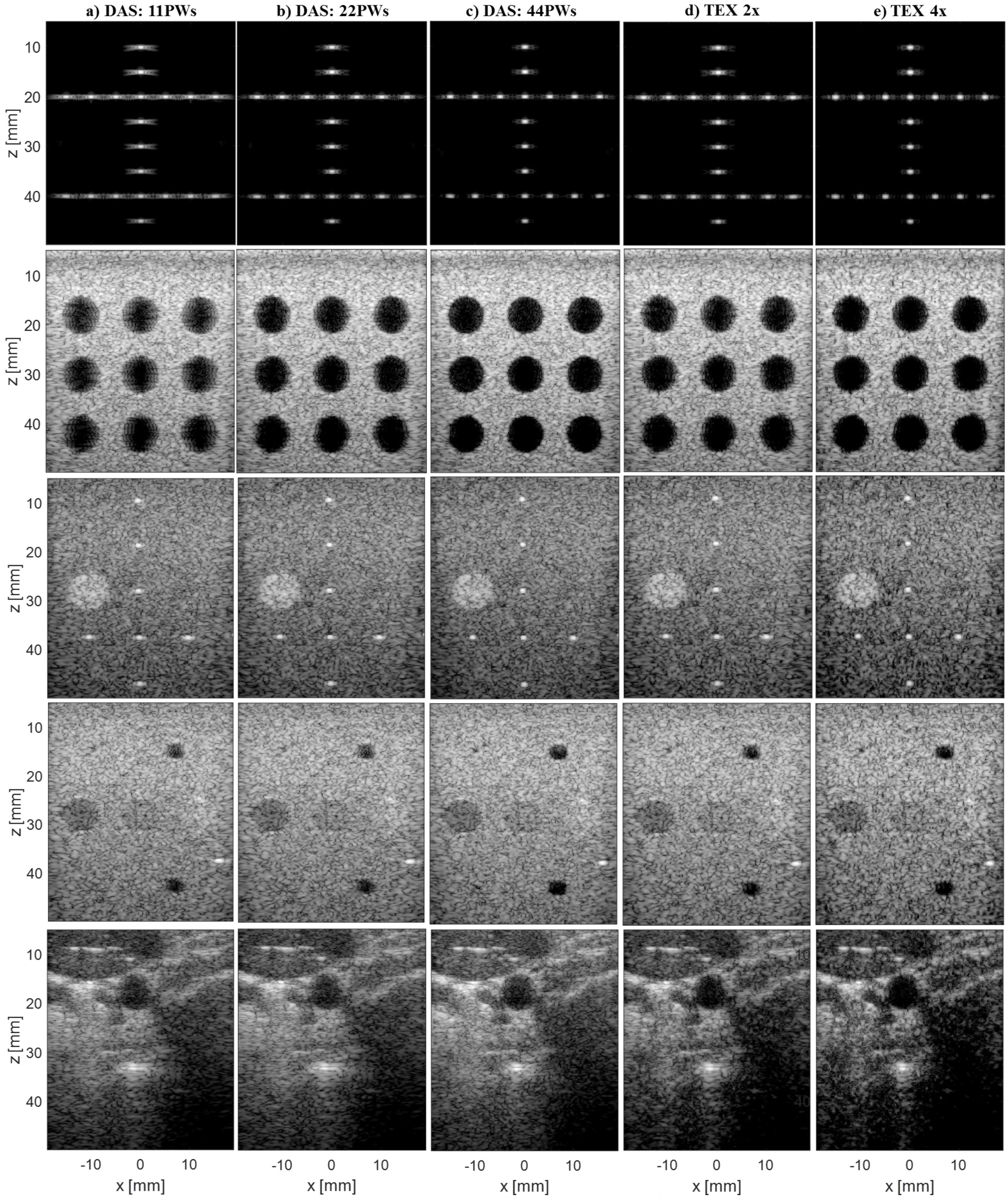

Fig 2. Results based on PICMUS dataset. Rows 1 and 2 show Field II simulations for point targets and anechoic cysts, respectively. Rows 3 and 4 show experimental phantom images for resolution and contrast evaluations, respectively. Row 5 shows *in vivo* human carotid data. Images are compared for coherent compounding of center a) 11 PWs, b) 22 PWs, c) 44 PWs, and for TEX with extrapolation factor of d) 2x (equivalent to 11×2=22PWs) and e) 4x (equivalent to 11×4=44PWs). All simulation and phantom images (rows 1-4) are displayed on 60 dB dynamic range and the in vivo images (row 5) are on 70 dB dynamic range.